Electronic Supplementary Information (ESI) for

Surface nanostructures for fluorescence probing of supported lipid bilayers on reflective substrates

Aleksandra P. Dabkowska,[a,b] Gaëlle Piret,[b,c,‡,º] Cassandra S. Niman,[b,c,‡] Mercy Lard,[b,c] Heiner Linke,[b,c] Tommy Nylander,[a,b] and Christelle N. Prinz,*[b,c,d]*

[a] Division of Physical Chemistry, Lund University, P.O. Box 124, SE-22100 Lund, Sweden

[b] NanoLund, Lund University, P.O. Box 118, SE-22100 Lund, Sweden

[c] Division of Solid State Physics, Lund University, P.O. Box 118, SE-22100 Lund, Sweden

[d] Neuronano Research Center, Lund University, SE-22184 Lund, Sweden

Experimental Section

Materials. All the lipids used in the study, including 1,2-di-(9Z-octadecenoyl)-3-trimethylammonium-propane (chloride salt) ($C_{42}H_{80}NO_4Cl$; 18:1 TAP; DOTAP), 1,2-dioleoyl-*sn*-glycero-3-phosphoethanolamine-N-(lissamine rhodamine B sulfonyl) (ammonium salt) ($C_{68}H_{109}N_4O_{14}PS_2$; Rhod-PE), and 1,2-dioleoyl-*sn*-glycero-3-phosphoethanolamine-N-(7-nitro-2-1,3-benzoxadiazol-4-yl) (ammonium salt) ($C_{47}H_{82}N_5O_{11}P$; NBD-PE) of >99% purity were purchased from Avanti Polar Lipids (Alabaster, AL). 5(6)- and 4-(2-hydroxyethyl)piperazine-1-ethanesulfonic acid (HEPES; ≥99.5%), sodium chloride (NaCl), (KCl), (Na_2HPO_4), (KH_2PO_4) were purchased from Sigma-Aldrich (Schnelldorf, Germany). Ethanol (99.7%) was purchased from Solveco AB (Rosersberg, Sweden). Chloroform (HPLC quality, 99.8% stabilized with ethanol) was purchased from VWR International (Leuven, Belgium). Water was purified to a resistivity of 18.2 MΩ·cm at 25 °C using the MilliQ system (Millipore). Buffers were filtered (0.2 μm syringe filter; Anotop 25 Plus, Whatman GmbH, Dassel, Germany) and degassed under vacuum prior to use.

Vertical nanowire fabrication. Vertically arrayed nanowires were grown on gallium phosphide (GaP) to the desired geometries as described previously.[1,2] GaP nanowires were grown vertically from gold particles randomly distributed by aerosol on polished (111)B GaP wafers (Grimet Ltd., Moscow, Russia) using metal organic vapor phase epitaxy (MOVPE) to produce nanowires with specific dimensions. Nanowire arrays were: (A) 0.04 nanowires per μm^2, 80 (±5) nm in diameter, nanowire lengths of 3.8 μm, and (B) 5.9 nanowires per μm^2, 65-140 nm in diameter, nanowire lengths of 3.0 (± 0.1) μm. All nanowire arrays were characterized by scanning electron microscopy (SEM) using a LEO SEM system (Zeiss).

Silicon oxide coating. Atomic layer deposition (ALD) was used to coat the GaP substrate with SiO_2 layers of specific thicknesses. ALD cycles (10, 30, 45, 60, 100 or 150 cycles) were deposited using an automated system (Fiji F200, Ultratech / Cambridge Nanotech Inc., Waltham, USA). Spectroscopic ellipsometry measurements were performed using the UVISEL-ER-AGAS Spectroscopic Ex-Situ Ellipsometer (SA Jobin Yvon-Horiba, France) at an incidence angle of 70° over a spectral range of 250 nm to 710 nm (stepsize of 10 nm). To determine the thickness of the deposited SiO_2, the recorded data was fitted to a model consisting of a SiO_2 layer[3] on top of native GaP-oxide on an infinitely thick GaP substrate.[4] The thickness of the native GaP-oxide was determined from a bare GaP wafer to 1.1 ± 0.1 nm and kept constant in the analysis of the subsequent SiO_2 layers. It was found that on average the deposition of each ALD layer of silane results in an average increase of the SiO_2 layer thickness of 0.11 ± 0.01 nm.

Particle deposition. All substrates were cleaned in chloroform and air-dried and plasma treated (Harrick Scientific, New York, USA) for 5 minutes immediately prior to use. In order to deposit silica particles at a sufficiently low surface coverage to identify individual particles, a solution (0.406 wt% SiO_2 content in water and particle diameter of 79 nm, as reported by the manufacturer) of ZL Snowtex (Nissan Chemical Industries, Ltd. Chiba-Prefecture, Japan) was flushed across the surfaces, which were subsequently rinsed with pure water and dried under nitrogen.

Formation of nanowire supported lipid bilayers. Small unilamellar vesicles were formed by the sonication method,[5] by first adding the aliquots of the desired amount of lipid from a stock solution in chloroform into a vial. The chloroform was evaporated under nitrogen flow, and trace amounts of solvent were removed under vacuum for 6 to 14 hours. The dry lipid film that was formed was rehydrated in buffer (to a final concentration of ≈1 mM), vortexed and left to stand for 30 minutes. The resultant lipid dispersion was sonicated until clear (30 seconds on, 30 seconds off for around 5 minutes) using a probe sonicator (Vibra-Cell, Sonics Materials Inc., Newton, CT), with the vial placed in a water bath to prevent over-heating of the sample. Any large aggregates and titanium particles from the sonicator tip were removed from the vesicle dispersions by centrifugation for 10 minutes at 6000 rpm. Vesicle diameters were determined to be around 50 nm (polydispersity of 0.22) using dynamic light scattering (Nanosizer, Malvern, Worcestershire, UK) at a lipid concentration of 100 μM, an angle of 173° and a temperature of 25 °C. To form lipid bilayers from vesicles, freshly cleaned surfaces were mounted in a disposable flow cell (sticky-Slide $I^{0.6}$ Luer, ibidi GmbH, Martinsried, Germany) and sealed with a cleaned coverslip. Lipid vesicles in buffer (500 μM) were injected into the flow cell to allow formation of a bilayer. The buffer in the flow cell was exchanged with at least twenty times the volume of the flow cell to remove excess vesicles from the bulk liquid.

To determine the presence of a lipid layer on the GaP surfaces, ellipsometry was performed on bilayers formed in a liquid cell at an incidence angle of 70° over a spectral range of 250 nm to 710 nm (stepsize of 10 nm). Briefly, a cleaned GaP surface was aligned in the liquid cell and submerged in water in order to characterize the surface. Next, a lipid bilayer was deposited as described above. Excess vesicles were rinsed off by exchanging the bulk liquid in the liquid cell with ten times the volume of water. The lipid layer was fitted by using the Cauchy model to express the wavelength dependence of the refractive index. Note that the wavelength dependence of refractive index within the used wavelength range was weak, and assuming a constant refractive index gave an equally good fit. The standard Horiba software was used to determine the refractive index and thickness of the layer to obtain the best fit to the experimental data.

Confocal microscopy. Imaging of the nanowire surfaces was performed using a Leica CLSM SP5 confocal microscope operated in the inverted mode using a 63x 1.2 numerical aperture water immersion objective or a 100x 1.4 numerical aperture oil immersion objective. The Rhodamine-labeled lipid probe was excited with a HeNe laser (543 nm) and detected using the fluorescence emission (560-700 nm). The temperature was controlled to be 20.0 ± 0.5 °C.

FLIC experiments. FLIC experiments were performed on lipid membranes supported on reflective surfaces. DOTAP bilayers fluorescently labeled with Rhod-PE (0.1 mol%) were deposited on clean surfaces with varying thicknesses of oxide produced ALD, as described above. For each DOTAP bilayer-coated GaP surface, images of 1024 x 1024 pixels captured using a 400 Hz bidirectional scan 1X zoom and the pinhole set to one airy unit. The gain was set to the same value (700V) for every image in the series while ensuring not to saturate any pixels in the image. The fluorescence intensity was quantified with ImageJ software (W. Rasband, National Institute of Health, Bethesda, MD, USA). Fluorescence intensities of bilayers deposited on different reflective surfaces were measured in at least three spatially separated regions in three independent samples. In every image, the mean pixel intensities in 30 square regions (each 5 μm by 5 μm) were measured, background-subtracted and averaged. The background was taken as the intensity in the bulk solution away from the surface.

FRAP experiments. FRAP experiments were performed on the CLSM using the FRAP application wizard in the Leica software. The field of imaging was about 40 μm x 40 μm (512 x 512 pixels). To determine the recovery over time, a time-lapse sequence of images was acquired. Prior to photobleaching, ten images taken in order to find the approximate initial fluorescence intensity of the ROI. Immediately after, a spot with a diameter of 3 μm was bleached with a ≈2 s pulse of the argon ion laser, set to a tube intensity of 80%. Subsequent images were taken of the fluorescence recovery every 0.645 s. Fluorescence intensity in the bleached area was then plotted as a function of time, background-subtracted and normalized to correct for differences in the starting intensity, the loss of total fluorescence due to photobleaching as well as differences in bleaching depth using the method of full scale normalization.[6]

As the beam profile is uniform and circular,[7] the fluorescence recovery time, τ_D, and immobile fraction, γ, were computed from the least squares fit performed in Mathematica of the normalized data to the function, *f(t)* as:

$$f(t) = (1-\gamma)\left[I_0\left(\frac{2\tau_D}{t}\right) + I_1\left(\frac{2\tau_D}{t}\right)\right]exp\left(-\frac{2\tau_D}{t}\right) \qquad \text{Eq. S1}$$

where t is time, and I_0 and I_1 are modified Bessel functions. Values for τ_D and τ with statistical p –value > 0.05 were excluded.

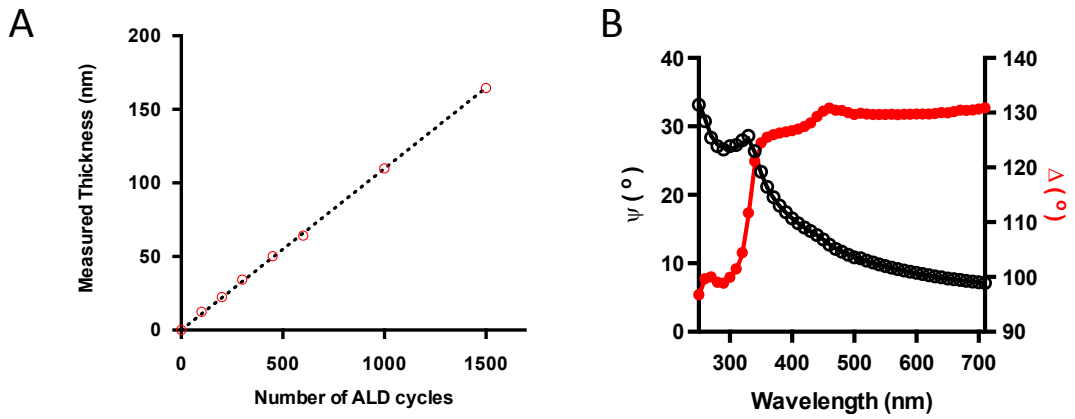

Figure S1. (**A**) Evolution of silicon oxide layer thickness with increasing number of ALD cycles, as determined by spectroscopic ellipsometry. (**B**) Spectroscopic ellipsometry data for 100 ALD cycles of SiO_2 deposition on GaP. The circles show the data for two ellipsometric angles, Ψ (black markers) and Δ (red markers), while the solid line shows the best fit according to the model described in the Experimental section.

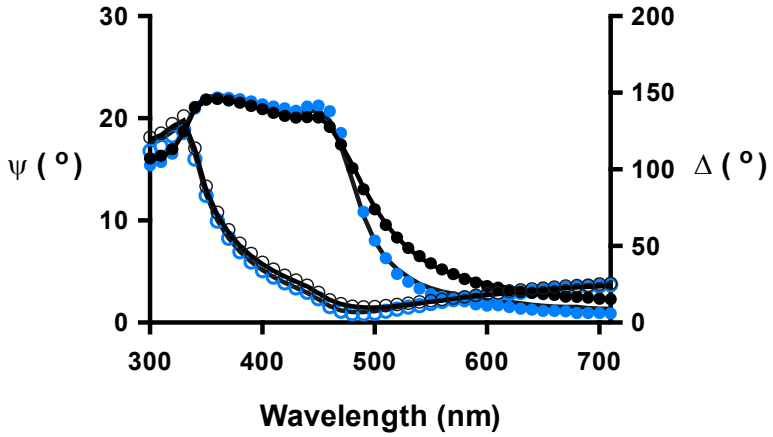

Figure S2. Changes in ellipsometric angles, Ψ (open markers) and Δ (filled markers) versus wavelength, for a bare GaP surface in water (blue markers) and after formation of a supported DOTAP lipid bilayer (black markers). The fitted thickness of the lipid layer was found to be 45 ± 5 Å, with a refractive index of 1.45 within the investigated wavelength range.

FLIC analysis. Theoretical FLIC curves reveal the variation with the same $\sin^2$ modulation for different heights of the lipid bilayer (fluorescent molecules) above the reflective surface including: 0, 4, 8, 16, and 32 nm (Fig. S3), see further[8]. These curves indicate that at SiO_2 heights greater than a few tens of nm, we expect to observe the

fluorescence of the bilayer (or any fluorescent molecule[9]) and as the distance between the probe from the SiO_2 substrate surface increases, the curve shifts to the left.

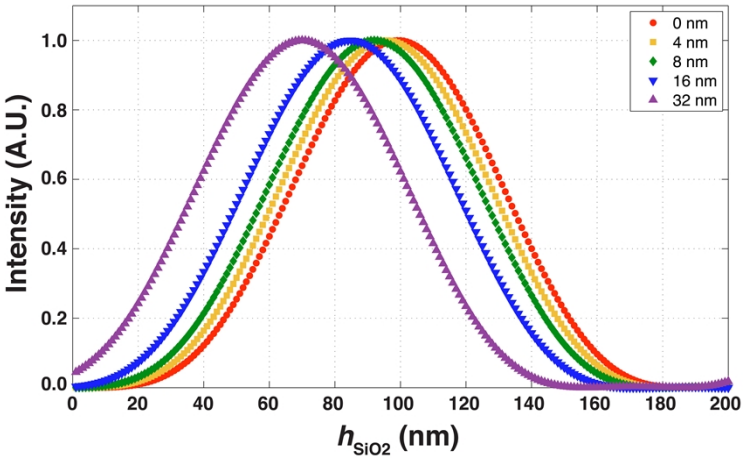

Figure S3. *Normalized* FLIC curves for SiO_2 based on Eq. 1. The TRITC filter set (ex/em = 543/628 nm) is used. Medium of immersion assumed to be water, with n_w = 1.333. Curves represent a shift in the relative intensity values with changing fluorophore heights.

Detection of the emission is an important parameter, where a clear shift in the relative intensity values is predicted when changing the emission wavelengths (Fig. S4).

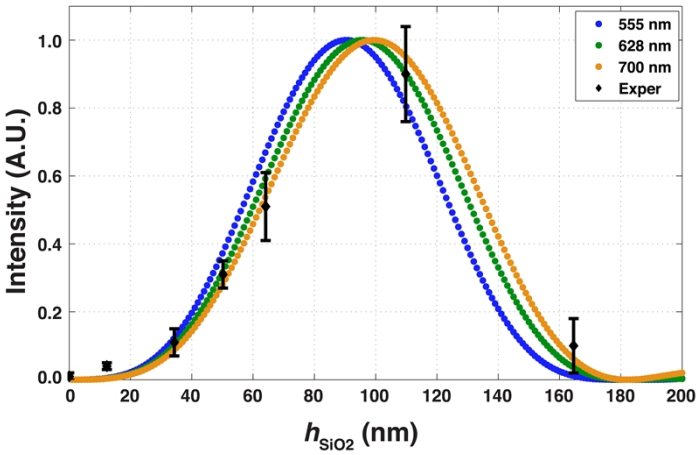

Figure S4. *Normalized* FLIC curves for SiO_2 based on Eq. 1. The TRITC filter set is used with varying emission wavelengths: (ex/em = 543/555 nm; blue), (ex/em = 543/628 nm; green), and (ex/em = 543/700 nm; orange). Fluorophore assumed to be 4 nm above the surface. Medium of immersion assumed to be water, with n_w = 1.333. Curves represent a shift in the relative intensity values with changing emission wavelengths. Black diamonds represent mean ± standard deviation (x; n = 3, y; n =10) pixel intensity and oxide thickness data on Rhod-PE labeled DOTAP bilayers and SiO_2 on GaP, respectively.

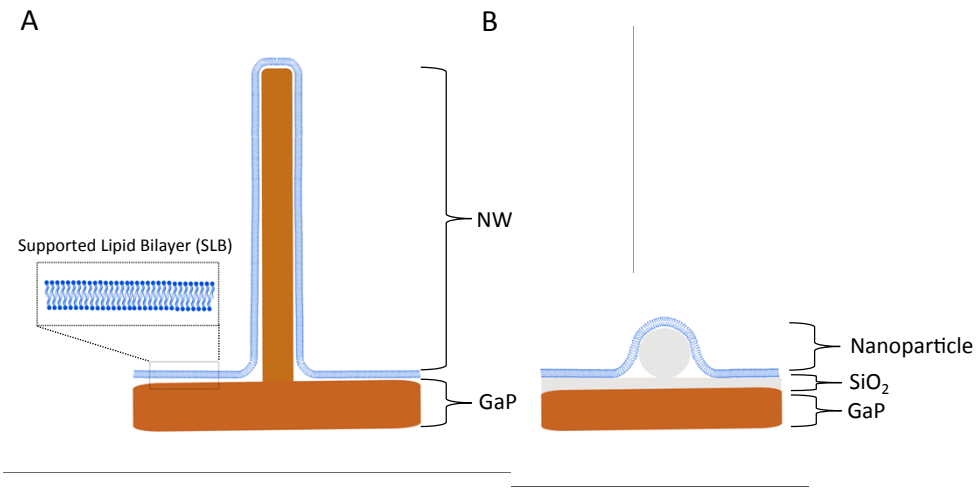

Figure S5. Schematic diagram of the surface nanostructures showing the FLIC geometry for SLBs on (**A**) vertically arrayed GaP nanowires and (**B**) deposited silica nanoparticles.

ESI References:

(1) Persson, H.; Køber, C.; Mølhave, K.; Samuelson, L.; Tegenfeldt, J. O.; Oredsson, S.; Prinz, C. N. *Small* **2013**, *9* (23), 4006–4016.
(2) Suyatin, D. B.; Hallstram, W.; Samuelson, L.; Montelius, L.; Prinz, C. N.; Kanje, M. *J. Vac. Sci. Technol. B* **2009**, *27* (6), 3092–3094.
(3) Philipp, H. R. *Handbook of Optical Constants of Solids*; Elsevier, 1997.
(4) Jellison, G.E., J. *Opt. Mater. (Amst).* **1992**, *1* (3), 151–160.
(5) Barenholz, Y.; Gibbes, D.; Litman, B. J.; Goll, J.; Thompson, T. E.; Carlson, R. D. *Biochemistry* **1977**, *16* (12), 2806–2810.
(6) Ellenberg, J.; Siggia, E. D.; Moreira, J. E.; Smith, C. L.; Presley, J. F.; Worman, H. J.; Lippincott-Schwartz, J. *J. Cell Biol.* **1997**, *138* (6), 1193–1206.
(7) Soumpasis, D. M. *Biophys. J.* **1983**, *41* (1), 95–97.
(8) Kiessling, V.; Tamm, L. K. *Biophys. J.* **2003**, *84* (1), 408–418.
(9) Lard, M.; ten Siethoff, L.; Månsson, A.; Linke, H. *Sci. Rep.* **2013**, *3*, 1092.